Electrical properties of amorphous Ge alloys and electron tunneling in amorphous semiconductors

J. J. Hauser
Bell Laboratories, Murray Hill, New Jersey 07974
(Received 30 October 1973)

The low-temperature resistivity of amorphous Ge-alloy films deposited at 77°K was well fitted by the relation $\rho = \rho_0 e^{(T_0/T)^{1/4}}$. The increase in the number of localized states resulting from an increase in the number of impurities is evidenced by a decrease in T_0. Impurities which lead to shallow energy levels in the crystalline form do not form localized states near the Fermi level while impurities with deep-lying levels do. Electron tunneling into various amorphous semiconductors (Ge, Ge alloys, Si, and InSb) resulted in qualitatively similar data: The tunneling conductance is nearly symmetrical in bias voltage and increases smoothly with voltage. The tunneling conductance exhibits the same temperature dependence as the conductance of the amorphous semiconductor. These tunneling experiments seem to indicate that the deep-level impurities increase the number of localized states within the mobility gap, while leaving the Fermi level essentially unchanged at the center of the pseudogap.

I. INTRODUCTION

The purpose of this paper is twofold: first to extend the previously published electrical conductivity data for amorphous Ge alloys[1] and present the pertinent sample analyses. Second, a rather extensive tunneling study into various amorphous Ge alloys was performed in order to determine the energy distribution of localized states in the pseudogap. The first tunneling of the type Al–Al_2O_3–amorphous-Ge was reported by Nwachuku and Kuhn[2] and disagreement was found in a later study by Osmun and Fritzsche.[3] More recent measurements by Smith and Clark[4] on Al–Al_2O_3–amorphous-Ge and on Al–Al_2O_3–amorphous-Si confirmed the results of Osmun and Fritzsche[3] and suggested that the first measurements[2] were erroneous because of an improper use of electronic differentiation. Finally, recent electron tunneling into amorphous Si using a silicon oxide barrier with a Pt counterelectrode by Sauvage, Mogab, and Adler[5,6] agreed with the results of both Osmun and Fritzsche[3] and Smith and Clark.[4] Furthermore, this latest study[5,6] reported that the conductance of the tunnel junctions had the same temperature dependence as that of amorphous Si without an oxide barrier. They[5,6] therefore concluded that the observed temperature dependence of the conductance can be interpreted in terms of tunneling into localized states within a mobility gap. Consequently, tunneling should be a most useful technique for the investigation of the localized impurity states.[1]

II. EXPERIMENTAL PROCEDURE

The experimental technique used in the deposition and in the electrical measurements of the amorphous semiconductor films was already briefly described in a preliminary report.[1] Furthermore, it is very similar to the technique used for amorphous-Ge films.[7] We shall therefore restrict the present description to modifications of the experimental technique not previously discussed. Almost all amorphous-alloy films of the present study were getter sputtered onto sapphire substrates held at 77 °K from a master-alloy target. Most targets were prepared from an arc-melted button[8] homogenized by stirring, which was then inductively molten in a graphite crucible. In some cases, when the impurity added to Ge could be obtained in a powder form which would cold sinter under pressure, the target was prepared by pressing a powder mixture of the desired concentration into the form of a button. This latter technique could only be used when the impurity (e.g., Sn) could be added in sufficient amounts (more than 20 at.%) to act as a binder for the Ge powder. Finally, certain alloy films were prepared by evaporating a small piece of a master alloy from a tungsten filament onto a sapphire substrate held at 77 °K. All the films were transferred under liquid nitrogen onto the resistivity holder which is then immersed in liquid helium. The resistivity of the film is then measured in helium gas by warming up to room temperature. The amorphous nature of the films was established by both electron and x-ray diffractions.

The tunneling junctions were prepared using the same geometry described for the transverse resistivity measurements of amorphous-Ge films.[9] A narrow Al strip (0.019 cm wide) is evaporated from a tungsten filament and oxidized for 15 min in dry oxygen at 125 °C. The amorphous-semiconductor film (Ge, Ge alloy, Si, or InSb) is then sputtered at 77 °K as a small disk 0.13 cm in radius. The counterelectrode is a Pb strip (0.019 cm wide) which is evaporated at 77 °K *in situ*, thus defining a junction with an active cross-sectional area of 3.6×10^{-4} cm^2. The junctions are then

TABLE I. X-ray fluorescence analysis of sputtering targets.

Nominal M conc. (at.%)		Ge counts[a]	M counts[a]	Fractional M counts	Experimental conc.[b] (at.%)
M = Ni	2	8203	508	0.058	3.3
	5	7896	918	0.104	5.9
	6.5	8000	844	0.095	5.4
	8.5	7743	1282	0.142	8
	10	8435	2060	0.196	11.1
	20	6440	4055	0.386	21.8
	30	4749	4669	0.496	28
	40	3752	9065	0.707	40[b]
M = Gd	5	10726	309	0.028	5
	10	8926	535	0.056	10[b]
M = Al	5	7104	38	0.0053	4.8
	10	7196	54	0.0074	6.7
	15	6897	120	0.017	15.4
	20	7023	162	0.022	20
	30	6798	245	0.035	31.8
	40	6750	313	0.044	40[b]
M = Sn	5	10090	5430	0.35	7.8
	10	9867	7974	0.45	10[b]
M = U	2	9871	1340	0.12	3.9
	5	8912	2858	0.24	7.7
	10	8469	3723	0.31	10[b]
M = In	5	12730	351	0.027	4.7
	10	9349	564	0.057	10
	20	7920	1020	0.114	20[b]
M = Tl	10	8872	294	0.032	...
	20[c]	9953	41	0.004	...
		6907	462	0.063	...
M = Pb	5	9600	257	0.026	8.4
	10	8840	367	0.040	12.9
	10	8015	484	0.057	18
	20	7778	507	0.062	20[b]
M = Bi	5	9667	98	0.010	3.9
	10	8781	227	0.025	9.8
	10	8395	221	0.026	10.2
	20	7298	397	0.051	20[b]

[a]These counts represent an average over the surface of the target, the deviation from the mean being less than 5%.

[b]The experimental concentration is obtained by assuming that the fractional M counts for the largest concentration studied correspond to the nominal concentration.

[c]This was a grossly inhomogeneous target showing a very coarse dendritic structure.

measured without warming up above 77 °K. The conductance-voltage curves were obtained by hand differentiating the I-V curves for the high-impedance junctions and by electronic differentiation for the low-impedance junctions. The junctions were measured by a four-probe technique which eliminates lead resistances.

III. EXPERIMENTAL RESULTS AND DISCUSSION

A. Sample analyses

As the solubility limit of most impurities is very limited in Ge, it is most important in such a study to verify the composition of the films and targets. Accordingly, the composition of the target and films was checked by x-ray fluorescence analysis and the results are shown in Table I. The comparison between experimental and nominal compositions is only a relative one as they have been set equal for the target with highest concentration. This choice was made on the basis that the x-ray fluorescence counts will be more accurate the higher the concentration. On the other hand, this is a poor choice from a metallurgical standpoint as the higher concentration targets are undoubtedly more inhomogeneous. At any rate, it is clear from Table I that either choice would lead to similar conclusions: If one excludes the low-melting heavy elements (Tl, Pb, Bi), most experimental concen-

trations are within ± 2 at.% from the nominal concentrations. The reason for the discrepancy found for Tl, Pb, and Bi could be the large difference in melting points between these elements and Ge, which results in a coarse segregation. This segregation was extremely bad in the case of the 20-at.%-Tl target as shown by the wide range of Tl counts in different areas of the target. It will be shown later that even when the x-ray fluorescence analysis does not exhibit large discrepancies (In and Bi) one may still have metallurgical difficulties with low-melting heavy impurities. As the targets are not Ge solid solutions because of the high impurity concentrations used (several at.%), the targets are composed of several intermetallic phases and are at best macroscopically homogeneous. Nevertheless, as sputtering is a steady-state process, the composition of the films should be fairly close to the average composition of the target. This was indeed found to be true by performing a Coprex analysis[10] on the Ge-Ni films and an atomic absorption analysis[11] on the Ge-Al films. In contrast with the x-ray fluorescence analysis, these two last-mentioned analyses provide an absolute measurement of the concentration. The results for the Coprex analysis on the Ge-Ni films shown in Table IIA reveal a composition somewhat lower than the nominal composition by at most 3 at.%. The same qualitative agreement is shown in Table IIB for the atomic absorption analysis on the Ge-Al films. The results of the x-ray fluorescence analysis on certain alloy films are listed in Table IIC. The experimental concentrations represent an absolute measurement in this case as the calibration for the fractional impurity concentration was obtained from the target measurement. Such a procedure is questionable as the films (which are on the average 6000 Å thick) are below the infinite thickness[12] required for Ge and the impurities. As this infinite thickness is different for different elements, a film with a given composition may not yield the same fractional count as the bulk of the same composition. Keeping this restriction in mind the x-ray fluorescence analysis on the films is still useful from two points of view. In the case of Ni and In there is good agreement between experimental and nominal concentrations. On the other hand, in the case of the heavy low-melting elements (Pb and Bi) the experimental concentration is two to four times larger than the nominal. As one shall see later these effects are reflected in the electrical properties. The reasons for the discrepancy found for the heavy low-melting elements could be twofold. The first difficulty is related to the low melting point, which results in a grossly inhomogeneous target as discussed above. Second, these elements have (because of their heavy atomic mass) a sputtering rate six times

TABLE II. Film analysis.

A. X-ray spectrochemical analysis (Coprex) of Ge-Ni films

Nominal Ni conc. (at.%)	Ni weight (μg)	Ge weight (μg)	Expt. Ni conc. (at.%)
2	1.85	195	1.2
5	4.85	196	3.0
10	8.87	146	7.0

B. Atomic absorption analysis of Ge-Al films

Nominal Al conc. (at.%)	Al weight (μg)	Ge weight (μg)	Expt. Al conc. (at.%)
5	50	8610	1.5
10	315	9565	8.1
15	415	9905	10.1

C. X-ray fluorescence analysis

Nominal M conc. (at.%)		Ge counts	M counts	Fractional M counts	Expt. conc.[a] (at.%)
M=Ni	5	3306	327	0.09	5.1
	10	2713	678	0.2	11.3
M=In	10	1468	79	0.051	8.9
	20	1126	173	0.133	23.3
M=Pb	10	1710	140	0.076	24.5
	20	1115	225	0.168	54.2
M=Bi	10	1294	147	0.10	39.2
	20	1268	193	0.13	51

[a]The experimental concentration is obtained as in Table I (e.g., for Ni 40 at.% corresponds to a fractional count of 0.707).

greater than Ge. Although sputtering is generally a steady-state process, this may not be true for such inhomogeneous targets made up with elements with very different sputtering rates. In conclusion, one can state that amorphous-alloy films with an impurity concentration less than 10 at.% (which as we shall see is the important concentration range for electrical properties) have a composition within ± 2 at.% from the nominal concentration of the target.

B. Electrical properties

The electrical properties of amorphous-Ge-alloy films were already discussed in a preliminary report[1]; we shall therefore only repeat briefly the few facts necessary for the comprehension of this paper and present more extensive data. The main conclusion from this study[1] was that impurities in amorphous-Ge films can be divided in two classes. Impurities which produce deep energy levels in the crystalline form of Ge (e.g., Cr, Ni, Cu, Pt, and Au) form localized states near the Fermi level in the amorphous films. On the other hand, impurities which produce shallow impurity levels (e.g., B, Al, Ga, In, As, Sb, Si, Sn, and Be) in the crystalline form do not form localized states near the Fermi level in the amorphous films. It was previously reported[7,9] that Ge films thicker than 300 Å sputtered and kept at 77 °K until measured have a low-field resistivity of the form

$$\rho = \rho_0 \, e^{(T_0/T)^{1/4}} \quad , \tag{1}$$

with $T_0 = 10^8$ °K. The fit is very good between 30 and 120 °K; above 120 °K the films anneal and T_0 increases as a result of annealing out localized states. The constant T_0 is given as[13]

$$T_0 = 16 \, \alpha^3 / k N(E_F) \quad , \tag{2}$$

where α is the coefficient of exponential decay of localized-state wave functions and $N(E_F)$ is the density of states at the Fermi level. If one uses $\alpha = 10^7$ cm^{-1}, the experimental value $T_0 = 10^8$ °K yields, from relation (2), $N(E_F) = 2 \times 10^{18}$ states/eV cm^3. One expects that the addition of an impurity which contributes a localized state near E_F will result via relation (2) in a decrease for T_0. This was qualitatively observed for Ge-Ni films,[1] where T_0 decreases from 10^8 °K for pure Ge to $\simeq 10^5$ °K as the Ni concentration was increased to 10 at.%. Using relation (2) with $\alpha = 10^7$ cm^{-1}, one can extract $N(E_F)$, which is plotted as a function of concentration in Fig. 1 as the solid dots.[14] It is evident from Fig. 1 that even for impurities like Ni, which contribute a localized impurity state above 6 at.%, hardly any localized state is formed below 6 at.%. A speculative explanation for this behavior was given in Ref. 1. Above 6 at.% the density of localized states $N(E_F)$ increases linearly with concentration and the slope of the line implies one localized state per eV per Ni atom or, in other words, one localized state in the pseudogap per Ni atom. This interpretation assumes that the change in T_0 is due to a change in the density of localized states $N(E)$ and not to change in the Fermi level (E_F). The tunneling experiments to be discussed later seem to indicate that E_F remains in the center of the gap for concentrations as high as 10 at.%. The annealing behavior of the films is strikingly different in the two concentration regions. In the low-concentration region, annealing at 300 °K leaves $N(E_F)$ essentially unchanged; furthermore, deposition at 300 °K yields approximately the same $N(E_F)$ as shown in Fig. 1 for Ge-Ni films. On the other hand, when $c > 6$ at.% annealing results in a large decrease of $N(E_F)$ and deposition at 300 °K results in still lower values. This annealing behavior suggests that upon annealing impurities are rejected in submicroscopic clusters of second phase, thereby reducing the number of localized states. The data of Daver *et al.*[15] on Ge-Cr films evaporated at 77 °K and annealed at 300 °K are shown in Fig. 1 and fall close to Ge-Ni films sputtered at 300 °K and somewhat below sputtered films annealed at 300 °K, thus demonstrating that one should not study annealed films as most of the impurities are no longer in solution. All impurities which form localized states near E_F (Cr, Ni, Cu, Rh, Pt, Au, Gd, and U) behave in the same manner as Ni. This is shown in Fig. 1 for Gd and Cr. The as-deposited data for Cr agree very well with the as-deposited Ni data and the annealed data agree with annealed Ni data and are close to the data of Daver *et al.*[15] (the difference between the two being ascribed to the difference between sputtered and evaporated films[1]). The results for Rh, Pt, and U agree with those shown in Fig. 1 but with slight differences. When the nominal concentration of these latter impurities is less than 5 at.%, they do not contribute localized states (less than 10^{20}). On the other hand, 2×10^{21} localized states are reached for nominal concentrations as low as 8 at.%. Although the scatter in $N(E_F)$ may seem large in the 6–10-at.% range it is quite reasonable in view of the fact that the composition of the films can only be determined to ± 2 at.%. Some amorphous-alloy films were deposited at 77 °K by evaporation. Although this is a simple way to make the films it does not provide the compositional accuracy of sputtering because of the different vapor pressures of various constituents. The Ge-Au and Ge-Cu films were obtained by evaporation and one can only state that above a concentration of approximately 5 at.% Au and Cu form localized impurity states near E_F as evidenced by the fact that $N(E_F)$ is about 10^{21} (eV cm^3)$^{-1}$ for concentrations around

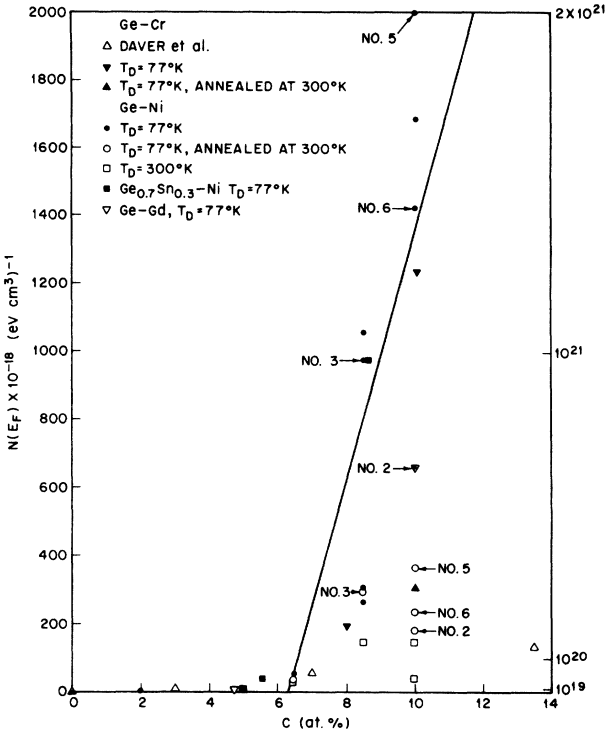

FIG. 1. Density of localized states obtained from $N(E_F) = 16\alpha^3/kT_0$, with $\alpha = 10^7$ cm^{-1}, as a function of impurity nominal concentration. The solid line corresponds to one localized state per eV per impurity atom above the critical concentration of $\simeq 6$ at.%.

10 at.%. Most of the impurities which formed localized states (Cr, Ni, Cu, Pt, and Au) are known[16] to lead to deep energy levels in the crystalline form.

We shall now turn our attention to the impurity atoms which do not result in a localized state near E_F, i.e., which did not result in an increase in $N(E_F)$ even for high impurity concentrations. Let us first consider the elements which are isoelectronic with Ge. Si did not form a localized state: The T_0 for a $Ge_{0.5}Si_{0.5}$ film[17] was 5.7×10^7 °K, which is between the values for pure Ge[7,9] (10^8 °K) and pure Si[17] (4.5×10^7 °K). This result is not surprising as Si has the same tetrahedrally coordinated diamond cubic crystal structure as Ge. In the case of Sn, there is essentially no increase in $N(E_F)$ up to 30 at.% as shown in Fig. 2. Figure 2 also demonstrates that this result is independent of film preparation, namely, sputtering of an alloy target (5 and 10 at.%), sputtering from a pressed-powder target (30 at.%), and evaporation (22 at.%). One can understand that Sn does not form a localized impurity state from the fact that amorphous-Ge-Sn films are homogeneous mixtures of Ge and Sn atoms in random tetrahedral coordination, as shown by x-ray diffraction and Raman scattering.[18]

As all impurities which do not contribute localized states near E_F yielded data similar to that shown for Sn in Fig. 2 or for Al (Fig. 3 of Ref. 1) the remaining data are summarized in Table III. Elements of column III (B, Al, Ga, and In) and column V (As and Sb), as well as Be did not form localized states. This is shown in Table III, where $N(E_F)$ for the highest concentration studied (which except for In is well in excess of 10 at.%) can be seen to remain extremely low as compared to impurities which form localized states (Fig. 1). Although there is no anomaly in the x-ray fluorescence analysis of the target (Table I) or of the films (Table IIC), a 20-at.%-In film became superconducting at 2.6 °K, which is a clear indication that such a film contained connected In filaments. As a result we could not analyze Ge-In films above 10 at.%. As mentioned previously, the metallurgical difficulties become even greater with Tl, Pb, and Bi. Again a 20-at.%-Pb film became superconducting at 2.7 °K. Because of these compositional difficulties, these films could not be trusted and one cannot ascertain whether or not Tl, Pb, and Bi form localized impurity states near E_F.

The fact that targets can be prepared by a pressed-powder technique (see $Ge_{0.70}Sn_{0.30}$ in Fig.

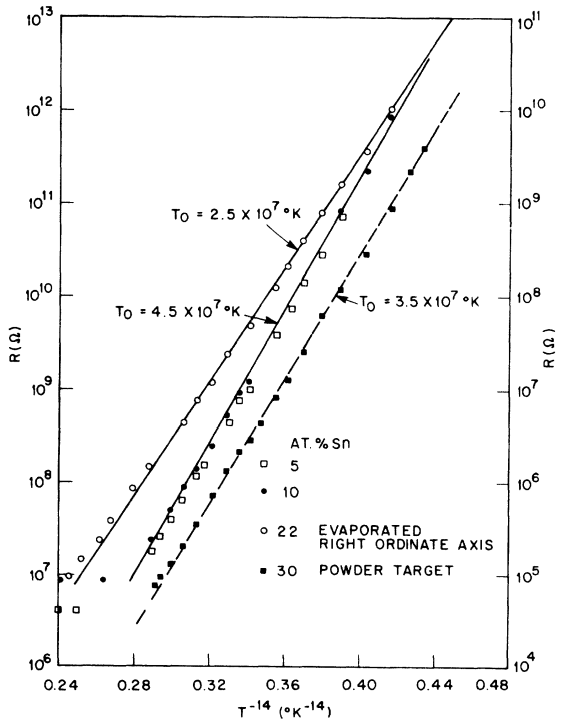

FIG. 2. Temperature dependence of the resistance for Ge-Sn films deposited at 77 °K with various Sn concentrations. The left ordinate axis applies to all samples except to the 22-at.%.

TABLE III. $N(E_F)$ for alloys with shallow-level impurities.

Impurity	Maximum conc.[a] (at.%)	Maximum $N(E_F)$[a] $(\text{eV cm}^3)^{-1}$
Si	50	3.2×10^{18}
Sn	30	5.3×10^{18}
Pb	...	...
Be	30	6.6×10^{18}
B	20	1.7×10^{19}
Al	40	4.6×10^{18}
Ga	20	1.8×10^{19}
In	10	2.8×10^{19}
Tl	...	...
As	30	4.5×10^{18}
Sb	30	3.2×10^{18}
Bi	...	...

[a]This is the maximum concentration which displays the temperature-dependent resistivity of relation (1) and the corresponding $N(E_F)$ obtained from relation (2).

2) leads to an interesting variation of the present study. Namely, as we have shown (Fig. 2) that Sn does not contribute a localized state, or in other words that Sn is germaniumlike, the effect of such an impurity as Ni should be the same in a Ge-Sn alloy as in pure Ge. This is indeed verified by the $Ge_{0.7}Sn_{0.3}$-Ni data shown in Fig. 1, which agree quite well with the Ge-Ni data. The $Ge_{0.7}Sn_{0.3}$-Ni films were sputtered from a pressed-powder target containing 30 at.% of Sn powder and various concentrations of Ni powder.

Although it is impossible to prepare Si alloys by melting in a graphite crucible because Si reacts with graphite, the pressed-powder technique offers an easy alternative. The data shown in Fig. 3 by the $Si_{0.7}Sn_{0.3}$ film which was sputtered at 77 °K from a pressed-powder target are well fitted by relation (1) with $T_0 = 1.2\times10^8$ °K. This value of T_0 corresponds via relation (2) to $N(E_F) = 1.5\times10^{18}$ $(\text{eV cm}^3)^{-1}$ and consequently Sn does not form localized impurity states near E_F in Si, just like in Ge. One can therefore study the behavior of an impurity in Si by using instead a Si-Sn alloy. This is shown for the case of Al in Fig. 3; there is very little change in T_0 with the addition of Al which indicates that Al does not form a localized impurity state near E_F in Si. Although the study with Si is rather brief, it would suggest that impurities will behave similarly in Si and in Ge and, consequently, that the localization behavior observed in the extensive study of Ge alloys would apply to most amorphous semiconductors. In conclusion, the concept of deep- and shallow-energy-level impurities is still meaningful in the amorphous state: deep-level impurities ($E > 0.1$ eV) form localized states near E_F while shallow-level impurities do not.

C. Tunneling into amorphous semiconductors

1. Generalities

We shall start this analysis by reviewing the pertinent tunneling experiments in amorphous semiconductors[2–6] and comparing them with the present results. While previous studies were restricted to amorphous Ge[2–4] and Si[4–6], tunneling experiments into amorphous InSb will be included as well. Finally, we shall discuss tunneling into amorphous Ge alloys and try to determine the distribution of localized impurity levels in the pseudogap. The first problem in a tunneling experiment is to demonstrate that the current flowing across the junction as a result of the applied bias voltage is truly a tunneling current and not some leakage current across pinholes in the oxide or similar artifacts. This question was partially answered by Osmun and Fritzche[3] and Smith and Clark[4] by simultaneously preparing three types of junction: MOSM, MOM, and one MSM (where M stands for metal, O for oxide, and S for amorphous semiconductor). The MSM junctions scaled with Ge thickness, indicating that the contacts were good and that there were no metal bridges or pinholes across the semiconductor. The MOM junctions served as quality check for the oxide layer. Tunneling was inferred from the fact that even at 77 °K the resistance of the MSM sandwich was several orders of

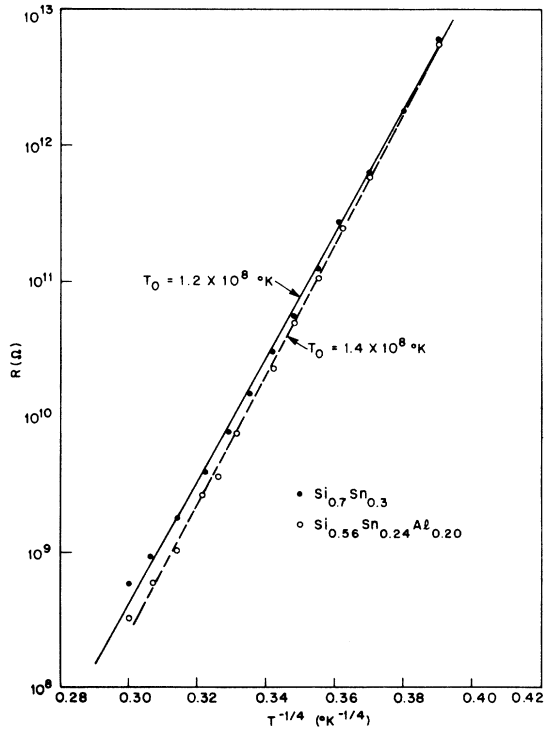

FIG. 3. Temperature dependence of the resistance for Si-Sn and Si-Sn-Al films deposited at 77 °K.

TABLE IV. Tunneling characteristics of amorphous-semiconductor junctions.

Sample[a]	d[b] (Å)	T_0 (°K)	ρ[c]	R[d] (77 °K, $V=0$)
Al-Ge-Al No. 1[e]	900	3.3×10^6	1.15×10^3	2.3×10^6
Al-Ge-Al No. 2[e]	900	4.7×10^6	1.17×10^2	2.5×10^6
Al-Ge-Pb No. 1[e]	900	2.5×10^6	•••	2.7×10^6
Al-Ge-Pb No. 2[e]	900	2×10^6	1.3×10^2	5.7×10^5
Al-Ge-Pb No. 3	900	2.5×10^6	9.3×10^2	10^5
Al-Ge-Pb No. 4	450	2×10^6	3.4×10^3	3.1×10^6
Al-Ge-Pb No. 5	240	2.3×10^6	3.5×10^3	3.9×10^6
Al-Ge-Pb No. 6	120	8×10^5	1.5×10^3	2.1×10^5
Al-Ge-Pb No. 7	30	•••	1.1×10^3	7.5×10^7
Al-Ge-Pb No. 8	15	•••	97	3.2×10^6
Al-Ge-Pb No. 9	10	•••	20	3500
Al-Ge-Pb No. 2	0	•••	1.2	4500
Al-Ge-Pb No. 3	0	•••	1.2	5300
Al-Si-Pb No. 1	660	1.2×10^6	8.5×10^2	4.1×10^5
Al-Si-Pb No. 4	330	•••	9.8×10^2	8×10^4
Al-Si-Pb No. 2	15	•••	2.3×10^3	5.6×10^7
Al-Si-Pb No. 3	10	•••	1.5×10^2	1.7×10^5
Al-Si-Pb No. 5[e]	200	4.2×10^7	•••	•••
Al-InSb-Pb No. 3	5400	6.5×10^6	4.2×10^2	4.5×10^4
Al-InSb-Pb No. 4	5400	6.5×10^6	2.7×10^3	4.8×10^4
Al-InSb-Pb No. 5	5400	8.8×10^5	•••	1.7×10^5
Al-InSb-Pb No. 6	4000	8.8×10^5	1.1×10^3	3.5×10^5
Al-InSb-Pb No. 1	2700	5×10^5	2.5×10^3	1.2×10^5
Al-InSb-Pb No. 2	225	1.1×10^5	8.8×10^3	3×10^4
Al-$Ge_{0.93}Pt_{0.07}$-Pb No. 1	3600	4.8×10^5	44	5000
Al-$Ge_{0.93}Pt_{0.07}$-Pb No. 3	60	•••	100	5500
Al-$Ge_{0.93}Pt_{0.07}$-Pb No. 2	30	•••	76	5000
Al-$Ge_{0.9}Ni_{0.1}$-Pb No. 2	3600	7.1×10^4	22	800
Al-$Ge_{0.9}Ni_{0.1}$-Pb No. 1	900	2.1×10^5	15	3000
Al-$Ge_{0.9}Ni_{0.1}$-Pb No. 3	900	1.3×10^5	42	1800
Al-$Ge_{0.92}Pt_{0.08}$-Pb No. 1	900	2.5×10^4	12	850
Al-$Ge_{0.9}Pt_{0.1}$-Pb No. 1	900	4.5×10^3	6	300

[a]The first electrode (Al) is thermally oxidized to produce the tunnel junction; the last electrode is the counterelectrode.

[b]Thickness of amorphous semiconductor.

[c]$\rho = R$ (77 °K, $V=0$)/R (77 °K, $V=1$ V).

[d]Junction resistance.

[e]Deposited at room temperature.

magnitude below that of the MOSM junction. The part played by the amorphous semiconductor in the tunneling process was demonstrated by observing that MOM junctions were only slightly bias and temperature dependent, while the MOSM junctions had a much larger resistance with a strong bias and temperature dependence. The same checking procedure was adopted in the present experiments. The fact that tunneling was indeed the conduction mechanism was further established by letting the thickness of the semiconductor tend to zero in a MOSM junction (where the last M was Pb) and observing the superconducting characteristic as well as the phonon structure of Pb below its superconducting transition temperature of 7.2 °K. The second problem in such MOSM junctions is that one must ensure that the applied bias is totally across the junction and not partially across the semiconductor film. Indeed, as the tunnel conductance increases markedly with bias voltage, the series resistance of the semiconductor, especially at 77 °K, can be significant. This problem has been solved in two different ways: Sauvage and Mogab[5] corrected for the voltage drop across the semiconductor by measuring the capacitance of the junctions, while Smith and Clark[4] restricted the thickness of the amorphous semiconductor so that the voltage drop across the semiconductor (known from the MSM sandwiches) was less than 5% of the total bias. We shall use this latter scheme in the present study. All the tunneling conductance vs voltage curves were found[2-6] to be nearly symmetric with respect to zero bias. While Osmun and Fritzsche[3] always found the conductance at nega-

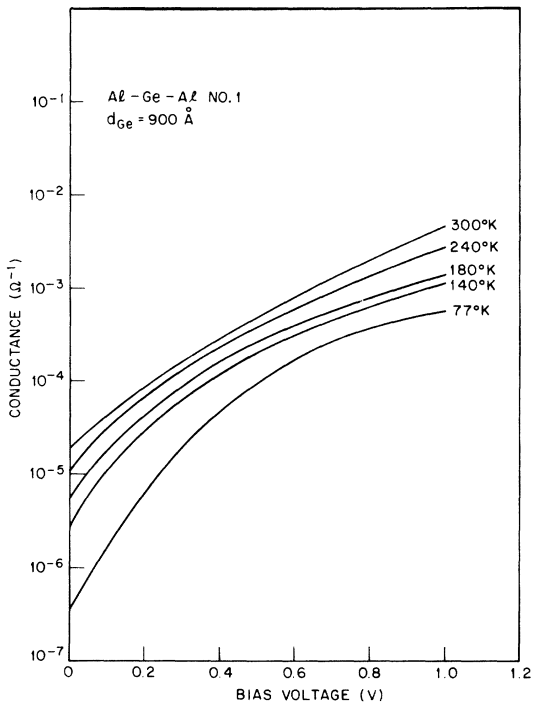

FIG. 4. Conductance as a function of bias voltage and temperature for an Al-Ge-Al junction deposited at 300 °K.

tive biases (meaning semiconductor negative) to be slightly higher than that at equal positive biases, just the opposite is found in the present study. However, Smith and Clark[4] have pointed out that this slight asymmetry depends on the oxide growth procedure and the oxide was formed by plasma oxidation in the case of Osmun and Fritzsche[3] and thermally grown in the present experiments. This slight asymmetry will therefore be ignored, and following Sauvage *et al.*[6] we will only show the positive-bias side of the curves. Furthermore, as most of the tunneling characteristics are very similar, only a few typical curves will be shown, while the important information taken from all tunneling curves is summarized in Table IV. Although most junctions were prepared by depositing the amorphous semiconductor at 77 °K, some junctions were prepared at room temperature in order to compare them with the existing literature.[2-6]

2. *Tunneling into amorphous Ge*

The conductance vs bias obtained by hand differentiation of the *I-V* curve is shown as a function of temperature for an Al-Ge-Al junction[19] in Fig. 4. In agreement with Osmun and Fritzsche[3] the change in conductance from 1-V to 0, bias is 10^3 at 77 °K and about 10^2 at 300 °K; the zero-bias conductance is about 10^2 times lower at 77 °K than 300 °K. Furthermore, while the zero-bias resistance of the MOM junction (Al-Pb) is typically 5000 Ω (Table IV), that of the MOSM junction prepared under identical conditions is, in agreement with Smith and Clark,[4] 10^2 to 10^4 times higher. It is also obvious from Table IV that the characteristics of such junctions remain essentially unchanged with different counterelectrodes (Pb instead of Al). Tunneling in such junctions is evident from the fact that the zero-bias resistance at 77 °K for the MOSM junction ($\simeq 10^6$ Ω) is several orders of magnitude higher than that of the corresponding MSM junction[9] ($\simeq 10^2$ Ω). Sauvage *et al.*[6] have plotted the temperature dependence of the zero-bias conductance by Osmun and Fritzsche[3] and by Smith and Clark[4] on Al-Ge-Al junctions; this plot is reproduced in Fig. 5. The present and previous data[3,4] can be seen to agree in two ways. First of all, the conductances are proportional to $e^{-T^{-1/4}}$ with approximately the same slope, and second, the two sets of data agree in order of magnitude although the methods of preparation of the junctions were quite different in all cases. Because of the similar temperature dependence displayed by the MOSM and the MSM junctions, Sauvage *et al.*[6] proposed that the tunneling problem was analogous to the hopping conduction within localized states as discussed by Mott.[20] The main differences between

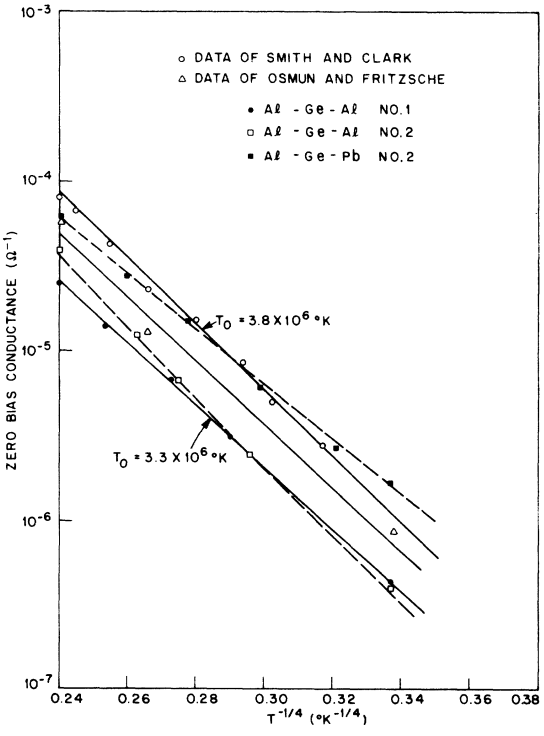

FIG. 5. Temperature dependence of the zero-bias conductance for Al-Ge-Al and Al-Ge-Pb junctions prepared at room temperature.

the two cases are the attenuation of the current by the tunnel barrier and a geometric factor that arises from the fact that tunneling occurs into a hemispherical region of the semiconductor. Accordingly, Sauvage *et al.*[6] proposed the following relation for the tunneling conductance:

$$\sigma = \sigma_0 \, e^{-(T_0/T)^{1/4}} \quad , \tag{3}$$

with

$$T_0 = 36 \, \alpha_s^3/kN(E) \tag{4}$$

and

$$\alpha_s = (2m^* \Delta E)^{1/2}/\hbar \quad , \tag{5}$$

where $\hbar$ is Planck's constant divided by 2π, m^* is the electron effective mass, and ΔE is the difference between the mobility edge and the applied bias. At zero bias, using parameters pertinent to Ge ($m^* = 0.1$ times the free-electron mass and $\Delta E = 0.4$ eV), $\alpha_s = 10^7$ cm^{-1}, which is the same as the value of α used in relation (2) for the conductivity measurements. The factor of 36 in relation (4) differs from the factor 16 in relation (2) because of the geometric factor mentioned above. Finally the prefactor σ_0 in relation (3) is essentially equal to $1/\rho_0$ [from relation (1)] multiplied by the probability factor for tunneling through the oxide barrier. Equation (3) implies that the logarithm of the tunneling conductance for biases below the mobility edge depends on temperature as $T^{-1/4}$, with a slope $T_0^{1/4}$ which should be slightly higher than that of the MSM junction if the density of states for the MOSM and MSM junctions are identical. Indeed, as will be shown later on, there is very good agreement between the values of T_0 obtained from MOSM and MSM junctions in the case of amorphous Si deposited at room temperature. Unfortunately, this agreement is by no means general. As shown in Fig. 5 and Table IV, although various junctions with room-temperature-deposited Ge seem to yield a T_0 of about 4×10^6 °K, this is significantly lower than the value of T_0 obtained from planar and transverse conductivity measurements[7,9] ($\simeq 10^8$ °K). We shall attempt to suggest a possible explanation for this discrepancy after examining more data. When the applied bias is equal to the mobility edge ($\Delta E = 0$), $\alpha_s = 0$ from relation (5), which means that one is tunneling into the extended states, at which point the tunneling conductance as given by relation (3) becomes, as expected, temperature independent. Indeed, Fig. 4 indicates that the conductance becomes progressively more temperature dependent below approximately 0.4 V and is essentially temperature independent above this value. The temperature dependence still present at 1 V, which is much larger than the temperature dependence of an Al-Pb junction, may be caused by some temperature dependence of the prefactor σ_0 in relation (3) which in turn results from the Al_2O_3 tunnel barrier modified by the presence of the Ge film. One can therefore identify 0.4 eV as the difference in energy between the Fermi level and the mobility edge, implying a mobility gap of about 0.8 eV for amorphous Ge, which is in fair agreement with other measurements (high-temperature resistivity and optical absorption). The symmetrical bias dependence of the tunneling conductance suggests a quasicontinuous distribution of localized states decreasing toward the Fermi level near the center of the gap. This is in contradiction both with the asymmetric model[20,21] and with the peak in the density of states at the Fermi level suggested by recent conductivity measurements.[22] This contradiction will be discussed with the T_0 discrepancy mentioned above as both problems may have a common origin. We shall now turn our attention to junctions where the amorphous semiconductor is deposited at 77 °K as this procedure is the only reliable one[1] for studying metastable amorphous Ge alloys.

In order to eliminate the Ohmic drop across the Ge film, the Ge film was decreased until the junction-resistance–vs–bias-voltage curve remained unchanged. By considering the ratio $\rho = R(77\,^\circ\text{K}, V = 0)/R(77\,^\circ\text{K}, V = 1\text{ V})$, this can be seen to occur around 450 Å (Table IV). One can notice from Table IV that junctions with Ge deposited at 77 °K are very similar to those with Ge deposited at 300 °K. The MOSM junction has a zero-bias resistance at 77 °K 10^2 to 10^4 times higher than that of the MOM junction and also several orders of magnitude higher than that of the corresponding MSM junction[9] ($\simeq$ a few ohms). The resistance at 77 °K decreases by a factor of 10^3 as the bias voltage increases from 0 to 1 V. The temperature dependence of the conductance is again well described by relation (3) with T_0 still having the low value of about 10^6 °K. One can observe that all this holds true as long as the Ge film remains thicker than 30 Å (although ρ decreases somewhat when $d \leq 120$ Å). Below 30 Å one expects the Ge film to be no longer continuous, but instead, to consist of isolated islands. This is evidenced by the 15-Å Ge junction where, although R is still high as a result of the Ge islands, the ratio ρ is appreciably lower, indicating that one is tunneling directly into Pb as well as tunneling into Ge. This effect is even more pronounced in the 10-Å Ge junction, where ρ had decreased even further, and where R is the same as for an Al-Pb junction, thus indicating that most of the tunneling takes place into the Pb. The presence of the Ge islands is however still clearly indicated by the strong bias dependence of this junction (ρ is still 20 as compared to 1.2 for an Al-Pb junction). The fact that tunneling is taking place in such junctions is well established by the

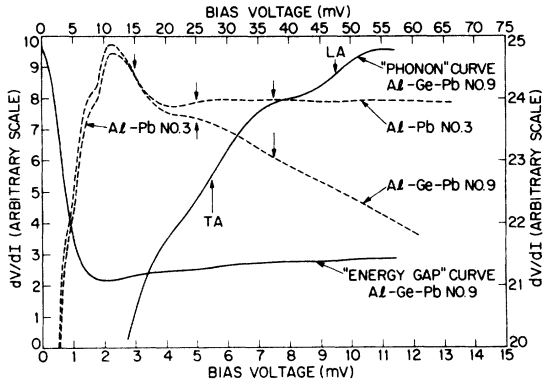

FIG. 6. Dynamic resistance (dV/dI) of an Al-Ge-Pb junction and an Al-Pb junction as a function of bias voltage measured at 4.2 °K. The two solid curves should be referred to the bottom abscissa axis with the "energy-gap" curve plotted vs the left ordinate axis and the "phonon" curve vs the right one. The two dashed curves should be referred to the top abscissa and right ordinate axes.

superconducting characteristics shown in Fig. 6. The "energy-gap" curve shows the proper characteristic for superconducting Pb with the correct energy gap $\Delta(4.2\ ^\circ\mathrm{K}) = 1.3$ mV.[23] Furthermore, a magnified plot (×8.8) of this curve referred to as the "phonon" curve clearly reveals the transverse (TA) and longitudinal (LA) phonon frequencies of Pb at the respective energies of 4.2 and 8.2 mV (after subtracting the gap energy of 1.3 mV), which are in good agreement with previous experimental values.[24] It is also obvious from Fig. 6 that the tunneling derivative for the Al-Ge-Pb junction is in very good agreement with the Al-Pb junction up to 20 mV; above this value the Al-Pb junction shows an essentially bias independent resistance, while the Al-Ge-Pb junction displays the strong bias dependence caused by the islands of the 10-Å Ge film.

The arrows at 15, 25, and 37.5 mV in the dashed curves of Fig. 6 are close to the structure at 8, 15, 25, and 35 mV reported by Ladan and Zylberstejn[25] (LZ) in Al-Ge-Sn junctions which they have ascribed to the phonon spectrum of amorphous Ge. They claimed[25] to have observed the effect by tunneling through a 30-Å-thick Ge film deposited at 77 °K between Al and Sn electrodes. First of all, if only the 30-Å film were present between the two electrodes, this would most probably have led to a short,[9] or at best, conductivity through such a film using $\rho(77\ ^\circ\mathrm{K}) \simeq 5000\ \Omega$ cm would yield a resistance of about 15 Ω, which is much lower than the 200- to 2000-Ω range observed by LZ at 77 °K. Furthermore, conduction through such a film (even if not continuous) should be strongly temperature and bias dependent as we have shown in the present study, in contradistinction with LZ's experiments. It would therefore appear that the effective tunneling barrier was not the amorphous Ge but instead a Ge-oxide layer formed as a result of warming up the Al-Ge films before depositing the Sn electrode. This would explain the structure at 70 mV as due to excitations of germanium oxide.[26] Although, as shown in Fig. 6, there is structure at 15, 25, and 37.5 mV in the Al-Ge-Pb junctions, these features are present as well in the Al-Pb junction and should therefore be ascribed to the Al rather than to the amorphous germanium. Finally, some of the structure observed by LZ[25] could also be ascribed to the Sn counterelectrode.

Previous studies[7,9] have shown that amorphous-Ge films deposited at 77 °K anneal around 120 °K and that the number of localized states decreases as a result of annealing. The same annealing effects are observed in tunnel junctions, as shown by Figs. 7 and 8. Figure 7 establishes that a tunnel junction with Ge deposited at 77 °K displays a reversible conductance-vs-bias-voltage curve as a function of temperature as long as one does not anneal it above 120 °K. On the other hand, the result of annealing a junction at 300 °K is shown in Fig. 8 to lead to two different separate effects. First of all, the general conductance level of the

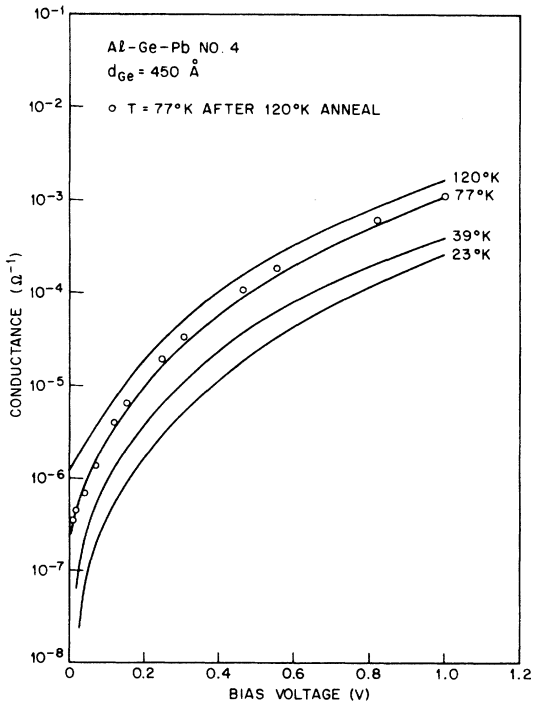

FIG. 7. Conductance as a function of bias voltage and temperature for an Al-Ge-Pb junction deposited at 77 °K showing the effect of 120 °K anneal.

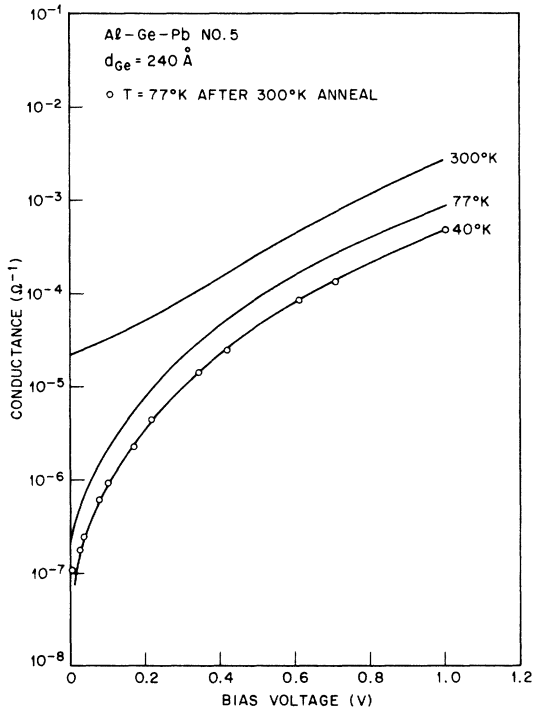

FIG. 8. Conductance as a function of bias voltage and temperature for an Al-Ge-Pb junction deposited at 77 °K showing the effect of 300 °K anneal.

junction decreases as a result of a change in the tunnel barrier. Second, the number of localized states has decreased, as evidenced by the ratio ρ, which increased from 3500 (Table IV) to 4500. Although this latter result agrees with expectations, it should be taken with caution, as it was pointed out above that the number of localized states obtained from the junction measurements does not agree with that from the conductivity measurements. In agreement with room-temperature-deposited junctions, the conductance of junctions deposited at 77 °K becomes appreciably temperature dependent below $\simeq 0.4$ V (Fig. 8), which is consistent with a mobility gap of 0.8 eV.

3. *Tunneling into amorphous Si*

The conductance-vs-bias-voltage curves are very similar to those obtained with Ge. For room-temperature-deposited junctions, the temperature dependence of the conductance shown in Fig. 9 can be seen to be in very good agreement with previous data.[4,6] Furthermore, the values of $(4-7)\times10^7$ °K obtained for T_0 in the tunneling experiments are in excellent agreement with values of T_0 [$(3-6)\times10^7$ °K] obtained in planar[17,27] and transverse[17] conductivity measurements. In other words, the density of states as obtained from the tunneling measurements [which Sauvage *et al.*[6] have established to be 5×10^{19} (eV cm^3)$^{-1}$ from relations (3)-(5) at zero bias] is in good agreement with bulk measurements. As can be seen from Table IV, this agreement is no longer true for tunnel junctions, where the Si film is deposited at 77 °K. The bias-voltage dependence of the conductance for such a junction, which is shown in Fig. 10, is qualitatively similar to the behavior of Ge tunnel junctions. The MOSM junction has a zero-bias resistance 10^2 to 10^4 times higher than that of the MOM junction and also several orders of magnitude higher than that of the corresponding MSM junction[17] (< 100 Ω). The resistance at 77 °K decreases by a factor of 10^3 (Table IV) as the bias voltage increases from 0 to 1 V. The annealing behavior of the Si tunnel junctions is somewhat different from the Ge junctions. While the general conductance level is again lower as a result of annealing (Fig. 10), the number of localized states seems to increase rather than decrease upon annealing as evidenced by the decrease of ρ from 850 (Table IV) to 180 (Fig. 10). This is consistent with the increase in the number of localized states upon annealing observed in the transverse conductivity measurements[17] which was shown to be the result of Pb diffusion into the amorphous-Si film. The temperature dependence of the conductance versus

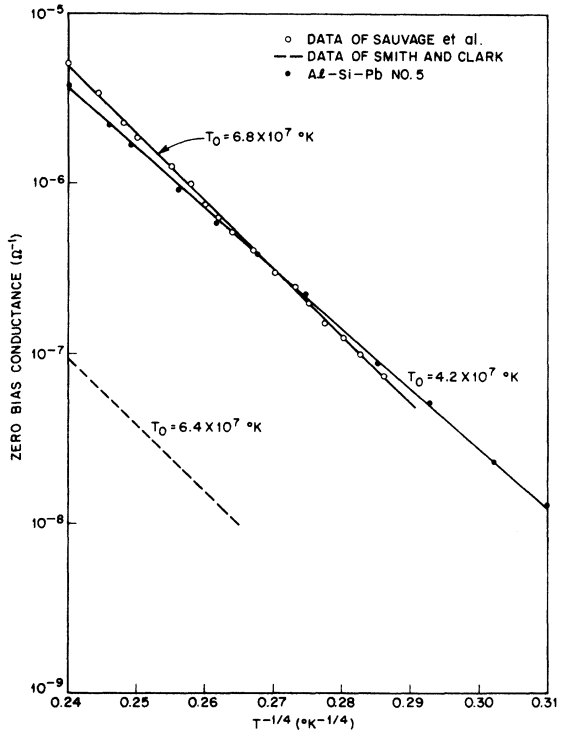

FIG. 9. Temperature dependence of the zero-bias conductance for various amorphous-Si tunnel junctions deposited at 300 °K.

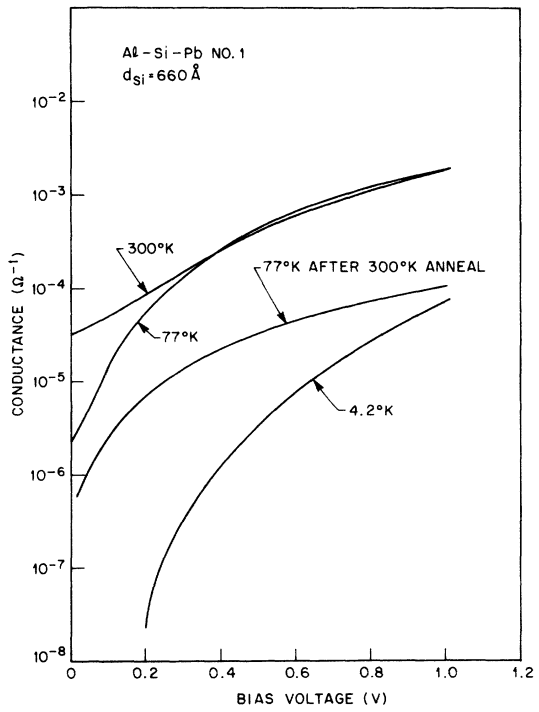

FIG. 10. Conductance as a function of bias voltage and temperature for an Al-Si-Pb junction deposited at 77 °K showing the effect of 300 °K anneal.

bias is again consistent with a mobility gap of 1 eV. Just as in the Ge case, the bias dependence of the junction decreases with decreasing film thickness. When the Si film is 10 Å thick, $\rho = 150$ (Table IV), the film is no longer continuous and as shown in Fig. 11 by the solid curve one observes the tunneling characteristic of superconducting Pb.

4. *Tunneling into amorphous InSb*

As the results for amorphous-InSb junctions are very similar to those obtained for Si and Ge, they will be dealt with very briefly. The tunneling characteristics summarized in Table IV clearly establish the tunneling process both by the high zero-bias resistance of the MOSM junction ($\simeq 10^5$ Ω) as compared to the MOM (3.5×10^3 Ω) and the MSM junction[28] ($\simeq 10$ Ω) and by the strong bias dependence ($\rho \simeq 10^3$) of the conductance. Once again, when the InSb film is sufficiently thin, one observes the superconducting characteristic of Pb (Fig. 11). One also notices in Fig. 11 that the superconducting energy gap of Pb is removed by the application of a 400 G magnetic field, which corresponds to the critical field of Pb at 4.2 °K. One should mention that the superconducting characteristic of Pb is observable with much thicker films of InSb (a few 100 Å) than with Si or Ge (a few 10 Å). This may be related to the fact that reliable transverse conductivity measurements could only be made with InSb films thicker than 5400 Å,[28] while one is able to push these measurements down to a thickness of 240 Å for Ge[7,9] and 610 Å for Si[17].

5. *Tunneling into amorphous Ge alloys*

As we are interested in the change of the tunneling characteristics with doping, we shall consider impurities which result in localized impurity states (such as Ni and Pt). Furthermore, as shown in Table IV, we shall only deal with concentrated alloys (7–10-at.% impurities) so as to obtain a large difference with undoped amorphous Ge. The first striking result that one observes in the tunneling characteristic of a doped Ge alloy is its "metallic" behavior: The zero-bias resistance of a junction with a doped Ge alloy is of the same order of magnitude as that of an MOM junction (Table IV). Nevertheless, the hopping conductivity of the amorphous-Ge alloy is still well evidenced by the strong bias dependence of such junctions: ρ as shown in Table IV has a value ranging from 6 to 100, as compared to 1.2 for an Al-Pb junction. The fact that the current through such junctions is truly a tunneling current is demonstrated by the fact that the zero-bias resistance of the MOSM junction, although comparable with that of the MOM junction, is still several orders of magnitude above that of the MSM junction (≃ fraction of an ohm). Furthermore, when the Ge-alloy film is thin (≃ 30 Å) one observes the superconducting energy gap of Pb (Fig. 11). The gap disappears at the superconducting transition temperature of Pb, where one is left with the strong bias dependence caused by the amorphous Ge alloy (compare

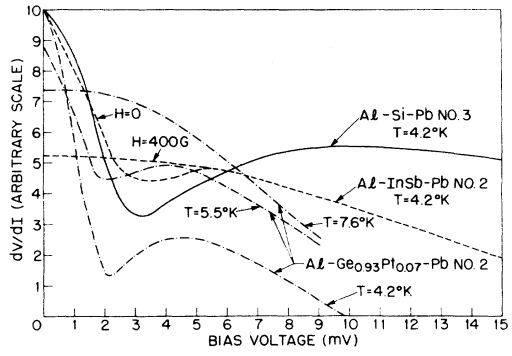

FIG. 11. Dynamic resistance (dV/dI) for an Al-Si-Pb junction (solid curve), an Al-InSb-Pb junction (dashed curves), and an Al-$Ge_{0.93}Pt_{0.07}$-Pb junction (dot-dashed curves) as a function of bias voltage. The Al-InSb-Pb derivative curves display superconductivity as a function of magnetic field while the Al-$Ge_{0.93}Pt_{0.07}$-Pb derivative curves display superconductivity as a function of temperature.

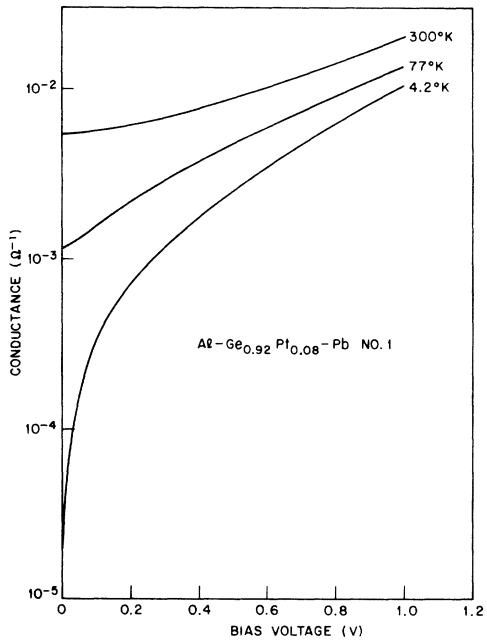

FIG. 12. Conductance as a function of bias voltage and temperature for an Al-$Ge_{0.93}$ $Pt_{0.07}$-Pb junction deposited at 77 °K.

Fig. 11 with the Al-Pb junction shown in Fig. 6). The bias dependence of the conductance for a typical amorphous-Ge-alloy junction is shown in Fig. 12. One should stress once again that just as for all other amorphous semiconductors, the conductance shown in Fig. 12 is symmetric with respect to bias voltage, thus implying that the Fermi level is approximately in the center of the pseudogap. Comparing Fig. 12 with, for example, Fig. 7, one concludes that although the conductance for the amorphous alloy is still strongly bias dependent ($\rho = 12$), the dependence is much weaker than in the case of undoped amorphous Ge ($\rho \simeq 10^3$). The fact can also be appreciated from Table IV, where it is shown that $\rho \leq 100$ for all alloys as compared to $\rho > 10^3$ for amorphous Ge. It is also apparent from Table IV that the temperature dependence of the zero-bias conductance is much weaker in the alloy case than for amorphous Ge: T_0 ranges from 5×10^5 to 5×10^3 °K for the alloys as compared to 2×10^6 °K for amorphous Ge. These two observations simply mean that in the alloy case the impurities (Ni and Pt) have contributed many localized states in the pseudogap. The temperature dependence of the conductance-vs-bias-voltage curves shown in Fig. 12 suggests that although some temperature dependence is present below 0.4 V (corresponding to a pseudogap of 0.8 eV), the major temperature dependence as shown by the 4.2 °K curve occurs below 0.2 V, suggesting that alloying has essentially reduced the mobility gap from 0.8 to 0.4 eV.

6. *Conclusions*

One may therefore summarize the situation in the following manner: In amorphous Ge (as in amorphous Si or InSb) the tunneling experiments seem to suggest that there exists a quasicontinuous distribution of states decreasing in density toward the Fermi level near the center of the pseudogap. Alloying seems to introduce localized states in the same symmetrical distribution as those already present, leaving the Fermi level in the center of the pseudogap at a minimum in the density of states. As the impurity states are more densely situated near the mobility edges, alloying also reduces the apparent mobility gap. Although the description presented here is quite self-consistent, the position of the Fermi level and the associated minimum in the density of states contradict previous models.[20–22] This contradiction may be disposed of, as Osmun and Fritzsche[3] already suggested, by noticing that states close to the surface may largely determine the tunneling process into amorphous semiconductors. In other words, if the asymmetric model[20,21] or the peak in the density of states at the Fermi level[22] would find confirmation for bulk amorphous semiconductors, one would have to conclude that the tunneling experiments only probe a thin surface layer from which conduction then proceeds by the transport processes of the bulk material. This speculation could also explain the discrepancy found between the values of T_0 [and therefore of $N(E_F)$] obtained from conductivity and tunneling experiments. In particular, except for the case of junctions with Si deposited at room temperature, the tunneling experiments of the present and past studies[3,4] always yield a lower value of T_0 (higher density of states) than the transverse conductivity measurements. This would be consistent with the fact that tunneling only probes the surface layer which conceivably contains more localized states (e.g., more dangling bonds). Of course, different amorphous semiconductors and different procedures of deposition of the same amorphous semiconductor, could result in different proportions of surface and bulk states, as we have observed in the case of amorphous Si.

ACKNOWLEDGMENTS

I would like to thank C. J. Mogab for discussing his experiments and J. M. Rowell for his suggestions on the (LZ, Ref. 25) tunneling experiments. I am indebted to J. Bernardini, D. Dorsi, Miss S. M. Vincent, and L. D. Blitzer for their able technical assistance.

[1]J. J. Hauser, Solid State Commun. 13, 1451 (1973).
[2]A. Nwachuku and M. Kuhn, Appl. Phys. Lett. 12, 163 (1968).
[3]J. W. Osmun and H. Fritzsche, Appl. Phys. Lett. 16, 87 (1970).
[4]C. W. Smith and A. H. Clark, Thin Solid Films 9, 207 (1972).
[5]J. A. Sauvage and C. J. Mogab, J. Non-Cryst. Solids 8–10, 607 (1972).
[6]J. A. Sauvage, C. J. Mogab, and D. Adler, Philos. Mag. 25, 1305 (1972).
[7]J. J. Hauser and A. Staudinger, Phys. Rev. B 8, 607 (1973).
[8]I am indebted to D. Dorsi for the preparation of the targets.
[9]J. J. Hauser, Phys. Rev. Lett. 29, 476 (1972).
[10]I am indebted to Miss S. M. Vincent for her help in the x-ray fluorescence analysis and for performing the Coprex analysis.
[11]I am indebted to L. D. Blitzer for the atomic absorption analysis.
[12]The infinite thickness is the thickness beyond which the x-ray fluorescence counts no longer increase.
[13]V. Ambegaokar, B. I. Halperin, and J. S. Langer, Phys. Rev. B 4, 2612 (1972).
[14]Figure 1 is essentially a repeat of Fig. 2 of Ref. 1 with more data included.
[15]H. Daver, O. Massenet, and B. K. Chakraverty, Solid State Commun. 11, 131 (1972).
[16]S. M. Sze, *Physics of Semiconductor Devices* (Wiley-Interscience, New York, 1969).
[17]J. J. Hauser, Phys. Rev. B 8, 3817 (1973).
[18]J. S. Lanin, Solid State Commun. 11, 1523 (1972).
[19]Throughout this paper Al-Ge-Al is used as a short hand for Al-Al_2O_3-Ge-Al; more generally the first electrode is thermally oxidized, the last one is the counterelectrode.
[20]N. F. Mott, Philos. Mag. 19, 835 (1969).
[21]N. F. Mott, Advan. Phys. 16, 49 (1967).
[22]M. Pollak, M. L. Knotek, H. Kurtzman, and H. Glick, Phys. Rev. Lett. 30, 856 (1973).
[23]This value of the energy is obtained by finding the bias voltage where $dV/dI = dV/dI$ (8 mV) as dV/dI (8 mV) is very close to the value of dV/dI when Pb is normal ($T > 7.2$ °K).
[24]J. M. Rowell, P. W. Anderson, and D. E. Thomas, Phys. Rev. Lett. 10, 334 (1963).
[25]F. R. Ladan and A. Zylbersztejn, Phys. Rev. Lett. 28, 1198 (1972).
[26]J. F. Scott, Phys. Rev. B 1, 3488 (1970).
[27]P. A. Walley, Thin Solid Films 2, 327 (1968).
[28]J. J. Hauser, Phys. Rev. B 8, 2678 (1973).